Yang et al. *IEEE* Magnetics Letters **8**, 3509504 (2017). **DOI:** 10.1109/LMAG.2017.2755587

Interfacial DMI Induced Directional Spin Wave in Spin-torque Oscillators

Long Yang[1], Philipp Dürrenfeld[1], Xuezhong Ruan[1], Wenqing Liu[1,2], Liang He[1], Yongbing Xu[1,2], and Yan Zhou[3*]

[1] *Jiangsu Provincial Key Laboratory for Nanotechnology, Collaborative Innovation Center of Solid-State Lighting and Energy-Saving Electronics, School of Electronic Science and Engineering, Nanjing University, Nanjing 210093, P.R. China*

[2] *York-Nanjing International Center of Spintronics (YNICS), Department of Electronics, The University of York, YO10 3DD, United Kingdom*

[3] *School of Science and Engineering, The Chinese University of Hong Kong, Shenzhen 518172, P. R. China*

* *Senior Member, IEEE*

Abstract

Spin torque oscillators (STOs) are currently of great interest due to its wide tunable frequencies, low energy consumption and high quality factors compared with traditional oscillators. Here, we report the characteristics of the nanocontact-(NC-)STO in the presence of interfacial Dzyaloshinskii-Moriya interaction (DMI), using micromagnetic simulations. We find that the DMI can decrease the STO frequency by around 2 GHz. More importantly, the DMI is able to break the isotropy of the spin-wave spectrum and turn the emitted microwave into directional spin-wave beams potentially facilitating the synchronization of multiple STOs.

Interfacial DMI Induced Directional Spin Wave in Spin-torque Oscillators

I. INTRODUCTION

Recently, the interfacial Dzyaloshinskii-Moriya interaction (DMI) in bilayers consisting of ferromagnet (FM) and heavy metal (HM) [Dzyaloshinsky 1958, Moriya 1960, Fert 1980] has attracted a considerable attention because it accelerates the magnetic domain wall movement [Thiaville 2012, Ryu 2014, Lee 2015] and provides a way to stabilize magnetic skyrmions at room temperature [Fert 2013, Zhou 2015]. Recent measurements have shown that a sizable interfacial DMI in thin permalloy ($Ni_{80}Fe_{20}$)/Pt bilayer system is present [Nembach 2015, Stashkevich 2015], which makes this system an interesting candidate for research in spintronic devices due to the widespread use of the low-damping $Ni_{80}Fe_{20}$. Spin torque oscillators (STOs) are spintronic devices [Flatte 2007], which generate radio frequency (RF) signals due to spin transfer torque (STT) [Berger 1996, Slonczewski 1996] induced magnetization oscillations leading to a time-varying magnetoresistance. STOs exhibit a large frequency tunability with current and magnetic field [Bonetti 2009], are intrinsically capable of being modulated [Pufall 2005], and have a drastically reduced footprint (less than 1 μm size for a single STO) compared with current LC tank–based RF oscillators. STOs are also potentially interesting for the implementation as read heads in high-density magnetic storage [Katine 2008].

In contrast to nanopillar-based STOs, which have a patterned magnetic fixed and free layer, in so called nanocontact- (NC-)STOs, the magnetic layers are left extended and the necessary high current densities are achieved by injecting the current through a point contact [Chen 2016]. In NC-STOs, a variety of spin wave modes can be excited in the extended magnetic film, such as localized spin wave bullets [Slavin 2005], propagating spin waves [Madami 2011], magnetic droplet solitons [Mohseni 2013], or dynamical skyrmions [Zhou 2015]. A transition from spin wave bullets to propagating spin waves is achieved by a strong out-of-plane component of the external magnetic field [Dumas 2013], where it was recently shown that the remaining in-plane component of the field together with the current-induced Oersted field lead to so-called propagating spin wave beams [Hoefer 2008, Houshang 2016]. These beams can strongly promote the synchronization of several NC-STOs [Kaka 2005, Mancoff 2005, Houshang 2016]. Recently, it was predicted that although interfacial DMI has a detrimental effect on the current-induced switching characteristics in a nanopillar [Jang 2015, Sampaio 2016], it promotes the directionality of spin waves [Brächer 2017]. STT-generated propagating spin waves under the influence of DMI have been numerically studied in spin Hall nano-oscillators, where a non-reciprocity of the spin waves was induced [Giordano 2016]. However, on one hand, these spin waves in spin Hall nano-oscillators have yet been only numerically predicted with an about twice as large threshold current compared with what spin Hall nano-oscillators can handle. On the other hand, NC-STOs and spin Hall nano-oscillators are two different devices with, for example, different Oersted field profile, applied fields, and current, so it is necessary to study the similar phenomena in NC-STOs. Experimentally, DMI in an NC-STO could be induced either purposefully or unintentionally by using, for example, platinum as the capping layer on the permalloy layer. Due to the technological relevance of propagating spin waves for information transport [Neusser 2009], it is important to explore how the generation and propagation of the spin wave could be

tuned by DMI. Here, we have studied the effect of an interfacial DMI on the spin wave characteristics in NC-STOs with a large out-of-plane magnetic field component by detailed micromagnetic simulations. We found that the DMI influences the STO frequency, power, and can break the isotropy of the spin-wave distributions.

II. MODEL AND DESCRIPTION

The energy of an interfacial DMI between two atomic spins $\boldsymbol{S}_i$ and $\boldsymbol{S}_j$ can be expressed as [Dzyaloshinsky 1958, Moriya 1960]

$$E_{DM} = \boldsymbol{D}_{ij} \cdot \left(\boldsymbol{S}_i \times \boldsymbol{S}_j \right) \tag{1}$$

where $\boldsymbol{D}_{ij}$ is the DMI vector given by $\mathrm{D} \cdot \hat{e}_z \times \boldsymbol{r}_{ij}$, in which D is the DMI parameter, $\hat{e}_z$ is the unit vector parallel to the asymmetry direction and $\boldsymbol{r}_{ij}$ is the position vector pointing from $\boldsymbol{S}_i$ to $\boldsymbol{S}_j$. In continuous thin films with out-of-plane symmetry breaking, DMI can be treated as an energy density [Bogdanov 2001]

$$\varepsilon_{DM} = D(m_z \frac{\partial m_x}{\partial x} - m_x \frac{\partial m_z}{\partial x} + m_z \frac{\partial m_y}{\partial y} - m_y \frac{\partial m_z}{\partial y}) \tag{2}$$

where m_x , m_y , and m_z are the normalized components of the magnetization vector.

The dynamics of the free layer are calculated by solving the Landau-Lifshitz-Gilbert (LLG) equation including a Slonczewski spin torque term

$$\frac{dm}{\mathrm{dt}} = -\gamma m \times H_{eff} + \alpha m \times \frac{dm}{\mathrm{dt}} + \gamma \frac{\eta}{2\mu_0 e M_s t_F} J m \times (m \times M) \tag{3}$$

where m is the unit magnetization vector of the free layer and M is the spin polarization direction of the incoming current from the fixed layer. H_{eff} is the effective field including DMI, Heisenberg exchange, magneto-crystalline anisotropy, magnetostatic, thermal, externally applied, and current-induced Oersted fields. γ is the gyromagnetic ratio and α is the Gilbert damping constant. The last term in Eq. (3) is the Slonczewski spin torque term where η is the polarization ratio. μ_0 is the magnetic vacuum permeability. M_s is the saturation magnetization, t_F is the thickness of the free layer, and J is the current density.

FIG. 1 HERE

To study the impact of DMI on STO performance, the magnetization dynamics of the free layer are simulated with the GPU-accelerated finite-difference solver Mumax3 [Vansteenkiste 2014]. The micromagnetic model of a Pt/$Ni_{80}Fe_{20}$/Cu/Co/substrate multilayer stack is adapted from Ref. [Houshang 2016] as shown in Fig. 1. However, we consider a thinner $Ni_{80}Fe_{20}$ free layer due to the appearance of DMI only in those systems. θ is the out-of-plane angle between the positive x-axis and the direction of the magnetic field. The magnetization direction of the polarized current is derived by solving the magnetostatic boundary conditions for a Co fixed layer assuming that the $\mu_0 M_s$ of Co is 1.7 T. Properties of the 1.3 nm thick $Ni_{80}Fe_{20}$ are set as $\mu_0 M_s$ = 0.775 T, exchange stiffness (A) of 10 pJ/m, and a weak perpendicular magnetocrystalline anisotropy (K_u) of 0.10423 MJ/m^3 according to [Nembach 2015]. A standard Gilbert damping factor (α) of 0.01 is considered. Experimental studies have shown that the interfacial DMI energy density in $Ni_{80}Fe_{20}$/Pt systems can reach values of well above 1 mJ/m^2 [Stashkevich 2015], and we here simulate values between 0 and 1.6 mJ/m^2.

We simulate a disk of 2048 nm in diameter, discretized by a two-dimensional mesh of cells with the size 2 nm × 2 nm × 1.3 nm. The spin-polarized current with η = 0.3 is applied to the centrally located NC of 100 nm diameter and the Oersted field around the NC is calculated via the Biot-Savart law and by approximating the current flow with an infinite cylinder. To avoid pseudo spin-wave reflections from the boundary of the computational disk, we initialize a series of increasing damping parameters from 0.01 to 1 within 12 nm at the calculative border as an absorbing boundary condition, which is similar to the abrupt absorbing boundary condition described in [Consolo 2007]. A random thermal field of standard normal distribution in time space, representing a temperature of 300 K is added to the simulations.

III. RESULTS AND DISCUSSIONS

We first analyze how DMI affects the frequency of the STO when current flows through it. Our simulation time is 10 ns, along with a time interval to save data every 0.01 ns so that we can evaluate the frequency of STO up to 50 GHz by Fast Fourier Transform (FFT). Due to the limitation of computer memory, we employ an FFT on m_y of each cell in the central square area 350 × 350 cells rather than the whole computational area. We use a Hanning window function for the time trace in each cell. The overall power spectral density (PSD) of the NC-STO is determined by an average of the FFT amplitudes over the cells and the peak frequency is determined from the position of the maximum of the PSD. The order of averaging the FFTs of the single cells is chosen to reduce the noise as well as to map the total power of the spin waves. Experimentally, e.g., by magnetoresistive measurements, one would be sensitive only to the spatial average of the magnetization near the NC and thus the relative phases of the single spins would have to be taken into account, leading to changes in the measured power.

FIG. 2 HERE

As shown in Fig. 2 (a), when current is varied from 3 mA to 11 mA, the frequency of STO oscillation increases almost linearly as a function of current. Hereby, we fix the magnetic field of 1 T to be pointing along 70° with respect to the film plane. This positive current tunability is a clear sign of the NC-STO emitting propagating spin waves, as intended. However, with an increasing DMI parameter, the

frequency of the STO descends by an amount of up to 2 GHz for $D = 1.6$ mJ/m^2. This shows a way to change the intrinsic STO frequency by selecting bilayers with different DMI parameters. For the total power of the STO, plotted in Fig. 2 (b), we integrate the PSD between ±2 GHz of the peak frequency. The power of the STO significantly reduces in the presence of DMI, which relates to smaller magnetization precession angles. An electrically measured signal would be up to 25% lower in power than without DMI. In this aspect, DMI is detrimental for practical STO devices.

FIG. 3 HERE

Next, we calculate the influence of DMI on the STO frequency when altering the magnitude and angle of the external field. We hereby fix the current to $I = 7$ mA. Both in Fig. 3(a) and in Fig. 3(b), the frequency also decreases when the DMI parameter becomes larger. The frequency shift can be as large as 2 GHz by means of considering DMI and remains relatively constant, independent of the magnetic field condition. Our reduction in frequency is in line with the numerical simulations of propagating spin waves in spin Hall nano-oscillators [Giordano 2016], yet we achieve a larger frequency difference mostly due to the larger applied field. We also notice that the STO still has a stable and uniform oscillation when $\theta = 90°$ in Fig. 3(b). Given the large magnetic field, the saturation magnetization, and the small perpendicular anisotropy of our free layer, the magnetization without the STT is perpendicular to the plane. However, the Co fixed layer is not saturated and leaves a finite angle between the fixed and free layer, thus resulting in an effective STT.

FIG. 4 HERE

In addition, we find that DMI affects the propagation of spin waves generated by the nanocontact. For this, we focus on the case of $I = 7$ mA and external fields of 0.6 T and 0.8 T, each at $\theta = 70°$. Fig. 4 shows the spatial distribution of the spin wave energy by plotting the local FFT amplitude of m_y at the peak frequency for each of the 350 × 350 central simulation cells. In Fig. 4(a) and 4(d), the spin waves propagate almost homogeneously from the central circle to the border without DMI. Yet, there is already an intrinsic anisotropic propagation of the spin waves to the top for $\theta \neq 90°$, initiated by the Oersted field from the current in the NC and its competition with the external field [Dumas 2013] and we will discuss this later. As the DMI parameter increases, the focusing of the spin waves in an upward direction increases, see Fig. 4(b). For the largest DMI parameter, the spin waves turn into beams just propagating towards the positive y-axis, see Fig. 4(c) and 4(f), with only a very small amplitude in the bottom side of the NC. In order to quantitatively discuss the asymmetry of the spin waves caused by DMI, we define an asymmetry parameter η_{asy}, which compares the FFT amplitudes of m_y (A) in the top and bottom halfs, and is expressed as

$$\eta_{asy} = \langle (A(x,y) - A(x,-y))^2 \rangle / \langle A(x,y)^2 \rangle \quad (4)$$

Hereby, the angle brackets mean the spatial averaging. The indices x and y are ranging from -175 to 175 ($x, y \neq 0$) and we additionally exclude the points located in the area of NC in order to only compare the propagating part of the spin waves away from the NC. The perimeter of the 100-nm diameter NC is shown in Fig. 4 as black circles. In this way, we derive η_{asy} only by analyzing the computational cells inside the central square 350 × 350 mesh yet outside the central circle mesh belonging to the NC.

TABLE 1 HERE

The defined asymmetry parameters η_{asy} of Fig. 4 are shown in TABLE I. n_{asy} is around 0.06 when $D = 0$ mJ/m^2 and η_{asy} increases to about 5 to 6 times as large values for 1.2 mJ/m^2, which shows that it is reasonable to use η_{asy} to describe the asymmetry of the spin waves along the y-axis. In the following, we will describe the relation of the asymmetry introduced by the Oersted field and DMI. We first get n_{asy} = 0.031 without the Oersted field in the case of Fig. 4(a), which is likely non-zero only due to the inclusion of thermal noise. Then n_{asy} increases to 0.067 when including Oersted field, showing that the Oersted field changes the symmetry of spin wave, but still being too small to see the asymmetry in the color plots in Fig. 4(a). Comparing with the Oersted field, the asymmetry introduced by the DMI is much larger in Fig. 4(c) and (f). It is notable, that reversing the in-plane component of the magnetic field results in both asymmetries to reverse and thus the spin wave propagates towards the bottom. This means, that here a positive D always promotes the spin-wave beam direction, whose asymmetry has already been established due to the Oersted field.

In addition, to target the cause of the additional asymmetry introduced by the DMI, we estimate the wave vectors of the spin waves going to the top and bottom when $x = 0$ nm. In a simulation with the same parameters as in Fig. 4(c), but with $T = 0$ K to avoid parasitic noise, we fit 10 snapshots of the magnetization with a damped sine-function. This gives an average of the wave vector and attenuation length along the y-axis. With this method, the average wave vector towards the top is 0.026 nm^{-1} and that towards the bottom is 0.098 nm^{-1} and thus considerably larger, in agreement with [Giordano 2016]. A large wave vector in thin metallic ferromagnets results in an increased effective damping [Li 2016], which in-turn hampers the spin wave propagation to the bottom, leading to a shorter attenuation length. The numerically estimated attenuation length towards the top is about twice as large as that towards the bottom.

IV. CONCLUSION

To summarize, we report that DMI can alter the frequency of a single STO overall when other conditions are the same. Although DMI is disruptive to the power of STO, we found that DMI can reduce the frequency by as much as 2 GHz. Moreover, spin waves play a key role in the synchronization of multi-STOs. Our results show that strong DMI can trigger directional spin-wave beams, which is expected to benefit the synchronization of the multiple STOs.

ACKNOWLEDGMENT

This work was supported by the National Basic Research Program of China (No. 2014CB921101), National Natural Science Foundation of China (No. 61274102, No. 61427812 and No. 11574137), The National Key Research and Development Program of China (No. 2016YFA0300803), Jiangsu NSF (BK20140054), Jiangsu Shuangchuan Programme, and Shenzhen Fundamental Research Fund under Grant No. JCYJ20160331164412545.

REFERENCES

Berger L (1996), "Emission of spin waves by a magnetic multilayer traversed by a current," Physical Review B, vol. 54, pp. 9353-9358, doi: 10.1103/PhysRevB.54.9353

Bogdanov A N, Rossler U K (2001), "Chiral symmetry breaking in magnetic thin films and multilayers," Phys Rev Lett, vol. 87, p. 037203, doi: 10.1103/PhysRevLett.87.037203.

Bonetti S, Muduli P, Mancoff F, Åkerman J (2009), "Spin torque oscillator frequency versus magnetic field angle: The prospect of operation beyond 65 GHz," Applied Physics Letters, vol. 94, p. 102507, doi: doi:http://dx.doi.org/10.1063/1.3097238.

Brächer T, Boulle O, Gaudin G, Pirro P (2017), "Creation of unidirectional spin-wave emitters by utilizing interfacial Dzyaloshinskii-Moriya interaction," Physical Review B, vol. 95, p. 064429, doi: 10.1103/PhysRevB.95.064429.

Chen T S, Dumas R K, Eklund A, Muduli P K, Houshang A, Awad A A, Dürrenfeld P, Malm B G, Rusu A, Åkerman J (2016), "Spin-Torque and Spin-Hall Nano-Oscillators," Proc. IEEE, vol. 104, pp. 1919-1945, doi: 10.1109/jproc.2016.2554518.

Consolo G, Lopez-Diaz L, Torres L, Azzerboni B (2007), "Boundary Conditions for Spin-Wave Absorption Based on Different Site-Dependent Damping Functions," IEEE Trans. Magn., vol. 43, pp. 2974-2976, doi: 10.1109/tmag.2007.893124.

Dumas R K, Iacocca E, Bonetti S, Sani S R, Mohseni S M, Eklund A, Persson J, Heinonen O, Åkerman J (2013), "Spin-Wave-Mode Coexistence on the Nanoscale: A Consequence of the Oersted-Field-Induced Asymmetric Energy Landscape," Physical Review Letters, vol. 110, p. 257202.

Dzyaloshinsky I (1958), "A thermodynamic theory of "weak" ferromagnetism of antiferromagnetics," Journal of Physics and Chemistry of Solids, vol. 4, pp. 241-255, doi: http://dx.doi.org/10.1016/0022-3697(58)90076-3.

Fert A, Levy P M (1980), "Role of Anisotropic Exchange Interactions in Determining the Properties of Spin-Glasses," Physical Review Letters, vol. 44, pp. 1538-1541, doi: 10.1103/PhysRevLett.44.1538.

Fert A, Cros V, Sampaio J (2013), "Skyrmions on the track," Nat Nanotechnol, vol. 8, pp. 152-6, doi: 10.1038/nnano.2013.29.

Flatte M E (2007), "Spintronics," IEEE Transactions on Electron Devices, vol. 54, pp. 907-920, doi: 10.1109/ted.2007.894376.

Giordano A, Verba R, Zivieri R, Laudani A, Puliafito V, Gubbiotti G, Tomasello R, Siracusano G, Azzerboni B, Carpentieri M, Slavin A, Finocchio G (2016), "Spin-Hall nano-oscillator with oblique magnetization and Dzyaloshinskii-Moriya interaction as generator of skyrmions and nonreciprocal spin-waves," Sci Rep, vol. 6, p. 36020, doi: 10.1038/srep36020.

Hoefer M A, Silva T J, Stiles M D (2008), "Model for a collimated spin-wave beam generated by a single-layer spin torque nanocontact," Physical Review B, vol. 77, p. 144401, doi: 10.1103/PhysRevB.77.144401.

Houshang A, Iacocca E, Dürrenfeld P, Sani S R, Åkerman J, Dumas R K (2016), "Spin-wave-beam driven synchronization of nanocontact spin-torque oscillators," Nat Nanotechnol, vol. 11, pp. 280-6, doi: 10.1038/nnano.2015.280.

Jang P-H, Song K, Lee S-J, Lee S-W, Lee K-J (2015), "Detrimental effect of interfacial Dzyaloshinskii-Moriya interaction on perpendicular spin-transfer-torque magnetic random access memory," Applied Physics Letters, vol. 107, p. 202401, doi: doi:http://dx.doi.org/10.1063/1.4936089.

Kaka S, Pufall M R, Rippard W H, Silva T J, Russek S E, Katine J A (2005), "Mutual phase-locking of microwave spin torque nano-oscillators," Nature, vol. 437, pp. 389-92, doi: 10.1038/nature04035.

Katine J A, Fullerton E E (2008), "Device implications of spin-transfer torques," Journal of Magnetism and Magnetic Materials, vol. 320, pp. 1217-1226, doi: http://dx.doi.org/10.1016/j.jmmm.2007.12.013.

Lee S-W, Park B-G, Lee K-J (2015), "Fast current-induced motion of a transverse domain wall induced by interfacial Dzyaloshinskii–Moriya interaction," Current Applied Physics, vol. 15, pp. 1139-1142, doi: 10.1016/j.cap.2015.06.023.

Li Y, Bailey W E (2016), "Wave-Number-Dependent Gilbert Damping in Metallic Ferromagnets," Phys Rev Lett, vol. 116, p. 117602, doi: 10.1103/PhysRevLett.116.117602.

Madami M, Bonetti S, Consolo G, Tacchi S, Carlotti G, Gubbiotti G, Mancoff F B, Yar M A, Åkerman J (2011), "Direct observation of a propagating spin wave induced by spin-transfer torque," Nat Nanotechnol, vol. 6, pp. 635-8, doi: 10.1038/nnano.2011.140.

Mancoff F B, Rizzo N D, Engel B N, Tehrani S (2005), "Phase-locking in double-point-contact spin-transfer devices," Nature, vol. 437, pp. 393-5, doi: 10.1038/nature04036.

Mohseni S M, Sani S R, Persson J, Nguyen T N A, Chung S, Pogoryelov Y, Muduli P K, Iacocca E, Eklund A, Dumas R K, Bonetti S, Deac A, Hoefer M A, Åkerman J (2013), "Spin Torque–Generated Magnetic Droplet Solitons," Science, vol. 339, pp. 1295-1298, doi: 10.1126/science.1230155.

Moriya T (1960), "Anisotropic Superexchange Interaction and Weak Ferromagnetism," Physical Review, vol. 120, pp. 91-98, doi: 10.1103/PhysRev.120.91.

Nembach H T, Shaw J M, Weiler M, Jué E, Silva T J (2015), "Linear relation between Heisenberg exchange and interfacial Dzyaloshinskii–Moriya interaction in metal films," Nature Physics, vol. 11, pp. 825-829, doi: 10.1038/nphys3418.

Neusser S, Grundler D (2009), “Magnonics: Spin Waves on the Nanoscale,” Adv. Mater., vol. 21, pp. 2927-2932, doi: 10.1002/adma.200900809.

Pufall M R, Rippard W H, Kaka S, Silva T J, Russek S E (2005), “Frequency modulation of spin-transfer oscillators,” Applied Physics Letters, vol. 86, p. 082506, doi: 10.1063/1.1875762.

Ryu K S, Yang S H, Thomas L, Parkin S S (2014), “Chiral spin torque arising from proximity-induced magnetization,” Nat Commun, vol. 5, p. 3910, doi: 10.1038/ncomms4910.

Sampaio J, Khvalkovskiy A V, Kuteifan M, Cubukcu M, Apalkov D, Lomakin V, Cros V, Reyren N (2016), “Disruptive effect of Dzyaloshinskii-Moriya interaction on the magnetic memory cell performance,” Applied Physics Letters, vol. 108, p. 112403, doi: doi:http://dx.doi.org/10.1063/1.4944419.

Slavin A, Tiberkevich V (2005), “Spin Wave Mode Excited by Spin-Polarized Current in a Magnetic Nanocontact is a Standing Self-Localized Wave Bullet,” Physical Review Letters, vol. 95, p. 237201.

Slonczewski J C (1996), “Current-driven excitation of magnetic multilayers,” Journal of Magnetism and Magnetic Materials, vol. 159, pp. L1-L7, doi: http://dx.doi.org/10.1016/0304-8853(96)00062-5.

Stashkevich A A, Belmeguenai M, Roussigné Y, Cherif S M, Kostylev M, Gabor M, Lacour D, Tiusan C, Hehn M (2015), “Experimental study of spin-wave dispersion in Py/Pt film structures in the presence of an interface Dzyaloshinskii-Moriya interaction,” Physical Review B, vol. 91, p. 214409, doi: 10.1103/PhysRevB.91.214409.

Thiaville A, Rohart S, Jué É, Cros V, Fert A (2012), “Dynamics of Dzyaloshinskii domain walls in ultrathin magnetic films,” EPL (Europhysics Letters), vol. 100, p. 57002, doi: 10.1209/0295-5075/100/57002.

Vansteenkiste A, Leliaert J, Dvornik M, Helsen M, Garcia-Sanchez F, Van Waeyenberge B (2014), “The design and verification of MuMax3,” AIP Advances, vol. 4, p. 107133, doi: 10.1063/1.4899186.

Zhou Y, Iacocca E, Awad A A, Dumas R K, Zhang F C, Braun H B, Akerman J (2015), “Dynamically stabilized magnetic skyrmions,” Nat Commun, vol. 6, p. 8193, doi: 10.1038/ncomms9193.

Figures

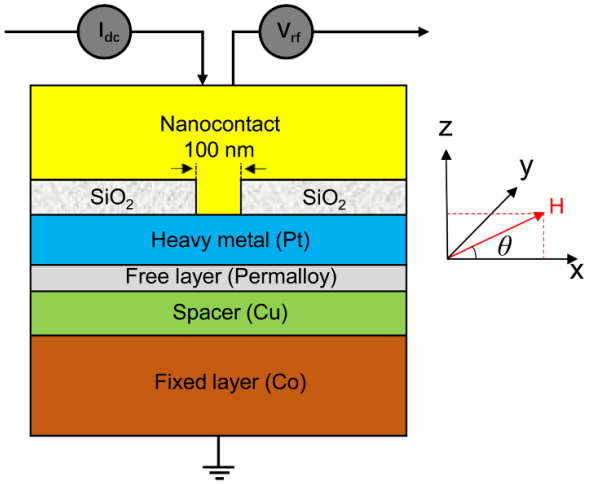

Fig. 1. Cross-sectional schematic of NC-STO based on Pt/$Ni_{80}Fe_{20}$/Cu/Co multilayer.

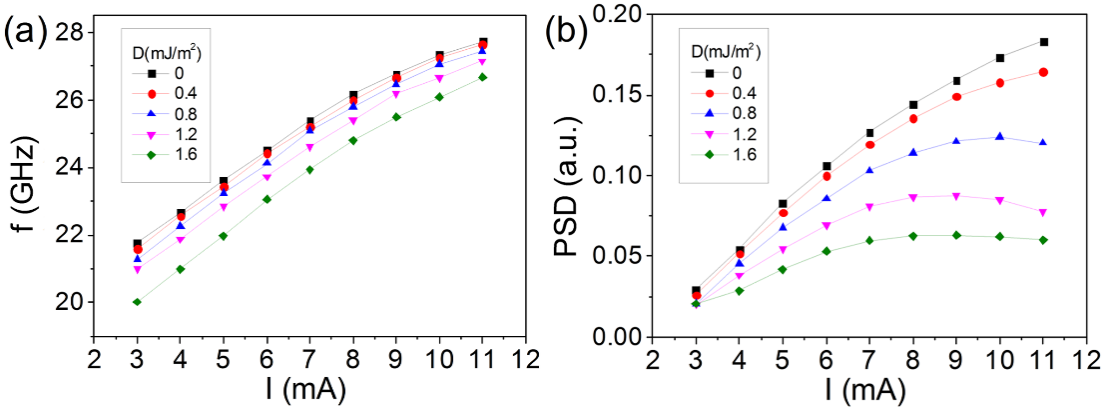

Fig. 2. (a) STO frequency as a function of the current for different DMI parameters. (b) Power of the STO as a function of the current for different DMI parameters. The angle of external field is 70° and the external field is 1 T.

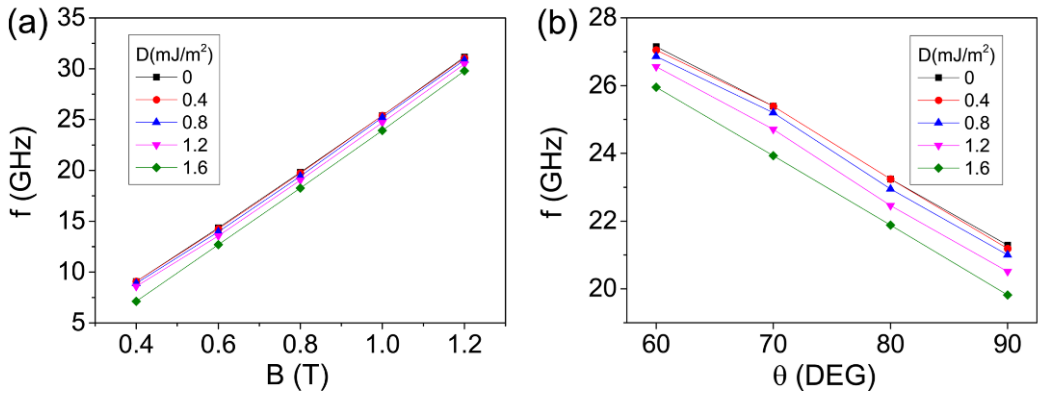

Fig. 3. (a) The STO frequency dependence on external field for different DMI parameters, where $\theta = 70°$ (b) The STO frequency dependence on the angle of external field for different DMI parameters where the external field is 1 T. The dc current is fixed to be 7 mA. θ is the angle between the external magnetic field and the film plane.

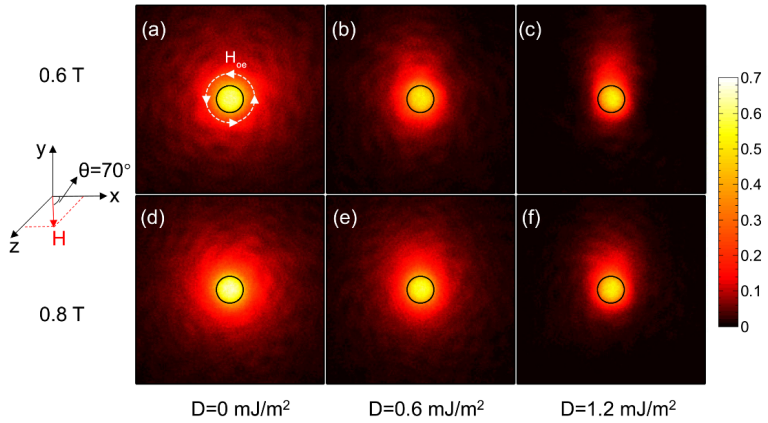

Fig.4. The simulated spin-wave propagation pattern excited by 7 mA dc current passing through the nanocontact along the positive z-axis with different DMI parameters D=0 mJ/m^2, 0.6 mJ/m^2, and 1.2 mJ/m^2 in [(a), (d)], [(b), (e)], [(c), (f)], respectively. The central black circle illustrates the boundary of the nanocontact and the colorbar is available for (a)-(f). The side length of each square picture is 7 times the contact diameter. The top panels correspond to the external field of 0.6 T while the bottom panels are plotted for the external field 0.8 T. The in-plane component of the external magnetic field points towards the positive *x*-axis and the direction of the Oersted field is only shown in (a).

	0 mJ/m^2	*0.6 mJ/m^2*	*1.2 mJ/m^2*
0.6 T	0.067	0.098	0.400
0.8 T	0.057	0.106	0.317

Table 1. Asymmetry Parameter of simulated spin wave patterns